$La_{0.8}M_{0.2}MnO_3$ (M=Ba, Ca, Ce, Mg and Sr) perovskite catalysts for plasma-catalytic oxidation of ethyl acetate

Xinbo Zhu[1], Xin Tu[2,*], Menghan Chen[1], Yang Yang[1], Chenghang Zheng[1], Jinsong Zhou[1], Xiang Gao[1,*]

[1] State Key Laboratory of Clean Energy Utilization, Zhejiang University, Hangzhou, 310027, China

[2] Department of Electrical Engineering and Electronics, University of Liverpool, Liverpool, L69 3GJ, UK

Corresponding author
Dr. Xin Tu
Department of Electrical Engineering and Electronics
University of Liverpool,
Liverpool, L69 3GJ
UK
Tele: +44-1517944513
E-mail: xin.tu@liverpool.ac.uk

Prof. Xiang Gao
State Key Laboratory of Clean Energy Utilization,
Zhejiang University,
Hangzhou, 310027,
P.R. China
E-mail: xgao1@zju.edu.cn

Abstract

Plasma-catalytic removal of low concentration ethyl acetate was carried out over $La_{0.8}M_{0.2}MnO_3$ (M= Ba, Ca, Ce, Mg and Sr) catalysts prepared by sol-gel method using citric acid as a mixing complex. The $La_{0.8}Ce_{0.2}MnO_3$ catalyst showed the highest removal of ethyl acetate and CO_2 selectivity over the specific energy density (SED) range followed by the $La_{0.8}Sr_{0.2}MnO_3$ catalyst, while Ba, Ca and Mg-doped catalysts inhibited the oxidation of ethyl acetate compared to the pure $LaMnO_3$ catalyst. A wide range of catalyst characterization including N_2 adsorption-desorption, X-ray diffraction (XRD), X-ray photoelectron spectroscopy (XPS) and temperature-programmed reduction by H_2 (H_2-TPR) indicated that the reducibility of the catalysts played an important role in determining the reaction performance of the plasma-catalytic gas cleaning process.

Keywords: Plasma-catalysis; Dielectric barrier discharge; Transition metal; Perovskite catalyst

1. Introduction

Volatile organic compounds (VOCs) are considered as a major contributor to air pollution and may cause health issues to humans. Great efforts have been devoted to the research and development of VOC abatement technologies in order to meet air quality standards [1]. During the last three decades, non-thermal plasma (NTP) technology has shown great potential for removal of low concentration VOCs in large volume waste gas streams due to its unique ability to generate a chemically reactive environment even at room temperature [2, 3]. However, the main disadvantages of NTP technology for the removal of VOCs are the formation of undesirable by-products in the plasma process and the relatively low energy efficiency. The combination of NTP and catalysis ("plasma-catalysis") provides a promising solution to overcome these problems. The interaction of the plasma and catalysts could generate a synergistic effect and affect the performance of plasma processing of VOCs, for example by improving the removal efficiency and CO_2 selectivity, and reducing the formation of by-products [4-6].

Up until now, various kinds of catalysts have been tested in the plasma-catalytic removal of VOC pollutants. Noble metal catalysts have shown excellent performance in VOC oxidation [7, 8]. However, the high cost and low poisoning resistance of noble metal catalysts limits their industrial application. Recently, transition metal catalysts have been intensively investigated due to their relatively low cost and poison resistance [4, 9, 10]. Among these catalysts, special attention has been paid to perovskite-type catalysts, especially $LaMnO_3$ catalysts due to their thermal stability, mixed valence states of the transition metals and oxygen mobility [11-13]. Dinh et al. reported that the removal efficiency of trichloroethylene was increased from 68% to 88% at a specific energy density (SED) of 460 $J \cdot L^{-1}$ in a two-stage plasma-catalysis configuration [14]. Vandenbroucke et al. also reported that the removal of trichloroethylene was improved by 25% when a $Pd/LaMnO_3$ catalyst was placed downstream of the plasma compared to that achieved when using plasma alone at a SED of 300 $J \cdot L^{-1}$ [15]. Partial substitution of the A-site in the perovskite structure of $LaMnO_3$ could change the catalyst structure and in turn affect the catalytic oxidation of pollutants including NO [16, 17],

chlorobenzene [11], vinyl chloride [18] and butane [19], etc. However, no work has been done on the use of A-site substituted $LaMnO_3$ catalysts in plasma-catalytic removal of VOCs. It is not clear about the roles of the substitutes in the plasma-catalytic oxidation process.

In this work, ethyl acetate was chosen as the model pollutant since it is widely used as a solvent in the chemical industry. A series of A-site substituted $LaMnO_3$ catalysts (M=Ba, Ca, Ce, Mg and Sr) were synthesized using sol-gel method and tested in a coaxial DBD reactor. Catalysts can be easily integrated into a DBD reactor as a hybrid plasma-catalytic process for the destruction of gas pollutants such as VOCs. In addition, DBD systems have been extensively used for ozone generation on an industrial scale and have great potential to be scaled up for the gas cleaning process. The role of the substitutes on the reaction performance was proposed based on the results of catalyst characterization.

2. Experimental

2.1 Catalyst preparations

The $La_{0.8}M_{0.2}MnO_3$ (M=Ba, Ca, Ce, Mg and Sr) perovskite type catalysts were prepared by sol-gel method using citric acid as the complexing agent. All chemicals were of analytic reagent grade. Metal nitrates were dissolved and mixed in deionized water to get solutions with the concentration of 0.1M. Then, citric acid with an excess molar ratio of 50% (compared to the total metal cations) was added to the above solution as a ligand. The solution was thoroughly stirred and evaporated in a water bath (80 ℃) to get viscous gel. The obtained sample was dried at 110 ℃ overnight and calcined at 700 ℃ for 5 h. The synthesized samples were sieved to 35-60 meshes. Pure $LaMnO_3$ was prepared using the same method.

2.2 Catalyst characterization

The N_2 adsorption-desorption experiments were carried out using a Quantachrome Autosorb-1 instrument at -196 ℃. The X-ray diffraction (XRD) patterns of the catalysts were analyzed by a Rikagu D/max-2000 X-ray diffractometer. X-ray photoelectron spectroscopy

(XPS) was conducted using a Thermo ESCALAB 250 instrument equipped with an Al Kα X-ray source at 150 W. Temperature-programmed reduction with hydrogen (H_2-TPR) was carried out using a gas chromatograph (Kexiao 1690) equipped with a thermal conductivity detector (TCD) to determine the reducibility of the samples.

2.3 Plasma-catalytic system

The details of the plasma-catalytic system have been described in our previous work [20]. A stainless steel mesh (ground electrode) 60 mm in length was tightly wrapped around of a quartz tube with an inner diameter of 8 mm and wall thickness of 1 mm. A stainless steel rod (2 mm in diameter) was used as a high voltage electrode and placed along the axis of the quartz tube. In each experiment, 100 mg of catalyst was packed inside the plasma region and held with quartz wool. The catalysts were pretreated in a N_2 flow for 1 h before each test. The DBD reactor was connected to an AC high voltage power supply (CTP-2000, Suman) at 10 kHz. The electrical signals of the plasma were recorded using a digital oscilloscope (Tektronix 4034B). The discharge power was calculated using the Q-U Lissajous method. The total gas flow rate was 1 L·min^{-1}, made up of 100 ppm ethyl acetate, 20% O_2 and N_2 in balance. Thus, the specific energy density (SED) was defined as:

$$SED(J \cdot L^{-1}) = \frac{P(W)}{Q(L \cdot min^{-1})} \times 60 \quad (1)$$

where P is the discharge power and Q is the gas flow rate.

The gas compositions (ethyl acetate, CO and CO_2) in the effluent were measured using a Gasmet Dx4000 FT-IR gas analyzer with an accuracy of ±3%. All measurements were carried out when the outlet gas composition reached equilibrium. The conversion of ethyl acetate ($\eta_{\text{ethyl acetate}}$) and CO_2 selectivity (S_{CO_2}) of the plasma-catalytic process were defined as:

$$\eta_{\text{ethyl acetate}} = \frac{c_{in} - c_{out}}{c_{in}} \times 100\% \quad (2)$$

$$S_{CO_2} = \frac{c_{CO_2}}{c_{CO} + c_{CO_2}} \times 100\% \quad (3)$$

where C_{in} and C_{out} are the inlet and outlet concentrations of ethyl acetate, respectively, while C_{co} and C_{co_2} are the concentration of outlet CO and CO_2.

3. Results and discussion

3.1 Structure of the catalysts

Table 1 summarizes the physicochemical properties of the $La_{0.8}M_{0.2}MnO_3$ catalysts. The specific surface area (S_{BET}) and pore volume of the $LaMnO_3$ catalyst were 14.4 $m^2 \cdot g^{-1}$ and 0.107 $cm^3 \cdot g^{-1}$, respectively. The substitution of La with the dopants slightly decreased the S_{BET} and pore volume except for the $La_{0.8}Ce_{0.2}MnO_3$ catalyst, which had a surface area of 17.0 $m^2 \cdot g^{-1}$ and a pore volume of 0.113 $cm^3 \cdot g^{-1}$.

The XRD patterns of the catalysts present the typical diffraction peaks of rhombohedral $LaMnO_3$ (JCPDS 50-0298) with characteristic peaks at 2θ=23.0°, 32.5°, 40.1°, 46.9°, 58.1°, 68.6° and 77.8° (**Fig. 1**). No obvious diffraction peaks for impurities like La_2O_3 and MnO_x were detected. The crystalline structure of $LaMnO_3$ was maintained after partial substitution of lanthanum. However, the main characteristic peak at 32.5° slightly shifted to a higher 2θ value when La^{3+} was substituted by Mg^{2+} and Ce^{4+}. This could be attributed to the difference in the ion radicals of these species as the ion radius of La^{3+} (1.06 Å) was larger than that of Mg^{2+} (0.71 Å) and Ce^{4+} (1.01 Å) [21]. Similarly, when La was substituted by ions with larger radius such as Ca^{2+} (1.14 Å), Sr^{2+} (1.32 Å) and Ba^{2+} (1.49 Å), the characteristic peak at 32.5° shifted to a lower 2θ value. This phenomenon also indicated the incorporation of the dopants into the perovskite lattice. The difference of ion radicals between La^{3+} and the dopants could change the lattice volume and form defects in the perovskite structure [22].

The particle size of the catalyst was calculated using Scherrer's equation based on the (200) crystal face at around 32.5°. The crystallite size of the catalysts decreased after partial substitution, while the $La_{0.8}Ce_{0.2}MnO_3$ catalyst showed the smallest crystal size of 14.0 nm. The crystallite size of other $La_{0.8}M_{0.2}MnO_3$ catalysts was in a narrow range of 15.9-16.6 nm, and followed the same trend as the ion radius. This phenomenon indicated that the crystalline

growth was restrained by the incorporation of the dopants, which was beneficial for the oxidation of VOCs over the catalyst surface.

3.2 Redox properties of the catalysts

The XPS spectra of O 1s are shown in **Fig. 1.** XRD patterns of the $La_{0.8}M_{0.2}MnO_3$ catalysts

Fig. 2. Three major components were identified by deconvoluting the peaks between 528 eV to 535 eV. The peak at 529.6 eV can be identified as lattice oxygen (O^{2-}) (denoted as O_{lat}), while that at 531.5 eV was assigned to the surface adsorbed oxygen (denoted as O_{ads}) [23]. The peak at 533.1 eV could be ascribed to surface adsorbed oxygen-containing species including hydroxyl and/or carbonate species on the catalyst surface. The molar ratio of O_{ads}/O_{lat} was calculated based on the area of the corresponding peaks and is given in **Table 1**. The addition of dopants increased the O_{ads}/O_{lat} value, while the $La_{0.8}Ce_{0.2}MnO_3$ catalyst exhibited the highest molar ratio of 47.5%.

The redox properties of the catalysts were analyzed using H_2-TPR from 100 to 800 ℃. For all the catalysts, two major reduction regions were observed. The first region was located between 250 and 500 ℃, while the second region was above 600 ℃. Moreover, a small peak was observed in the range of 150 to 250 ℃, which could be ascribed to the physically adsorbed oxygen species on the catalyst surface. For the pure $LaMnO_3$ catalyst, the first reduction peak at 304 ℃ can be attributed to the reduction of surface oxygen species, while the second peak could be ascribed to the reduction of Mn^{4+} to Mn^{3+}. The broad reduction peak above 600 ℃ was associated with the further reduction of Mn^{3+} to Mn^{2+} [11]. The presence of the dopants slightly changed the reduction behavior of the A-site substituted catalysts. The first reduction peak shifted to lower temperatures of 285 ℃ and 293 ℃ for the Ce and Sr doped catalysts, indicating a better oxygen mobility in these samples compared to pure $LaMnO_3$. By contrast, the first reduction peak for the Ba, Ca and Mg doped catalysts appeared at 315 ℃, 350℃ and 307 ℃, respectively. The H_2 consumption of the catalysts was calculated based on the H_2-TPR profiles. After A-site substitution, the H_2 consumption of the catalysts below 600 ℃ were between 3.73

μmol·g^{-1} and 5.26 μmol·g^{-1} - higher than that of the $LaMnO_3$ (3.53 μmol·g^{-1}) catalyst. The $La_{0.8}Ce_{0.2}MnO_3$ catalyst had the highest H_2 consumption of 5.26 μmol·g^{-1}. The reduction of Ce^{4+} to Ce^{3+} may occur in the reduction process considering ~50% higher H_2 consumption of the $La_{0.8}Ce_{0.2}MnO_3$ catalyst compared to that of the pure $LaMnO_3$ as the reduction of pure CeO_2 occurred at around 540 ℃ [20, 24]. Combining the lower reduction temperature and larger H_2 consumption, it can be deduced that the $La_{0.8}Ce_{0.2}MnO_3$ catalyst possessed the best reducibility among the tested catalysts.

3.3 Ethyl acetate removal

Fig. 4 shows the effect of different catalysts on plasma-catalytic removal of ethyl acetate in terms of the conversion of ethyl acetate and CO_2 selectivity. Clearly, the combination of the plasma and catalysts significantly enhanced the removal of ethyl acetate and the CO_2 selectivity. Note that these catalysts showed no activity towards the conversion of ethyl acetate at room temperature without plasma. The conversion of ethyl acetate increased with increasing SED regardless of the catalyst composition. It is well accepted that higher SED favours the generation of more energetic electrons and reactive radicals in the plasma [25]. These species are beneficial for the initiation of plasma-induced reactions and consequently oxidize ethyl acetate and its intermediates to the final products including CO, CO_2 and H_2O, etc. [4, 26]. For the pure $LaMnO_3$ catalyst, the ethyl acetate conversion increased from 64.2% to 90.5% when increasing the SED from 353.7 J·L^{-1} to 495.9 J·L^{-1}, 45 minutes after the initiation of the discharge the temperature at the reactor wall had increased and reached a stable state at about 83 ℃, even at a SED of 495.9 J·L^{-1}, indicating no significant thermal catalytic reactions occurred under the experimental conditions. The conversion of ethyl acetate in the plasma-catalytic process was slightly improved by partial substitution of La with Ce and Sr. The highest ethyl acetate conversion of 94.2% was achieved when placing the $La_{0.8}Ce_{0.2}MnO_3$ catalyst in the plasma at a SED of 495.9 J·L^{-1}, while this value was 92.9% for the plasma reaction over the $La_{0.8}Sr_{0.2}MnO_3$ catalyst at the same SED. By contrast, the presence of Ba, Ca and Mg species in the $LaMnO_3$ perovskite structure inhibited the oxidation

of ethyl acetate. The conversion of ethyl acetate was 86.8%, 85.9% and 89.0% for the Ba, Ca and Mg-doped $LaMnO_3$ catalysts, respectively. The CO_2 selectivity increased from 43.0% to 47.1% when increasing the SED from 353.7 $J \cdot L^{-1}$ to 495.9 $J \cdot L^{-1}$ for pure $LaMnO_3$. The combination of plasma and the modified $LaMnO_3$ catalysts slightly increased the CO_2 selectivity. At a SED of 495.9 $J \cdot L^{-1}$, the presence of the $La_{0.8}Ce_{0.2}MnO_3$ catalyst in the DBD showed the highest CO_2 selectivity of 54.4%, followed by Sr, Ca, Mg and Ba doped $LaMnO_3$ catalysts.

Obviously, enhancement in reaction performance was obtained in the combination of plasma and $La_{0.8}M_{0.2}MnO_3$ catalysts compared to using $LaMnO_3$. In such a plasma-catalytic system, plasma is mainly responsible for the generation of a highly oxidative environment consisting of chemically reactive species. Plasma-assisted surface reactions also played an important role in the oxidation of the pollutants as ethyl acetate, intermediates and reactive species could be adsorbed onto the surface of catalysts. After adsorption, the ethyl acetate molecules underwent a series of complex reactions to be converted to the final products [27]. Hot spots might have also been formed on the catalyst surface in the plasma reaction, accelerating the plasma driven surface reactions [5, 28]. Thus, the enhanced reaction performance when using $La_{0.8}Mn_{0.2}MnO_3$ catalysts can be mainly attributed to the modification of physicochemical properties of the catalysts in the presence of the dopants. The XPS results also showed the relative content of O_{ads} was increased by partial substitutions of La compared to that of $LaMnO_3$. The highest O_{ads} concentration of 47.5% was observed in $La_{0.8}Ce_{0.2}MnO_3$. Although the physicochemical characteristics of the $La_{0.8}M_{0.2}MnO_3$ catalysts were well maintained after the partial substitution of La based on the results of BET and XRD, electron compensation effect may have occurred to keep the neutrality of the perovskite structure as La^{3+} was substituted by ions with different valence or ions radius [18]. As a result, oxygen vacancies and defects may have formed on the catalyst surface, leading to a higher $O_{ads}/(O_{ads}+O_{lat})$. The release of surface oxygen species was much easier on catalysts with higher $O_{ads}/(O_{ads}+O_{lat})$. This could be further confirmed by the H_2-TPR as the $La_{0.8}Ce_{0.2}MnO_3$ catalyst exhibited the lowest reduction temperature of 285 ℃ followed by the $La_{0.8}Sr_{0.2}MnO_3$ and

$LaMnO_3$ catalysts, indicating $La_{0.8}Ce_{0.2}MnO_3$ was more easily reduced compared to other catalysts. It is noteworthy that a good correlation between the reaction performance and the reducibility of the catalysts was observed.

4. Conclusions

Plasma-catalytic removal of ethyl acetate over $La_{0.8}M_{0.2}MnO_3$ (M= Ba, Ca, Ce, Mg and Sr) catalysts was carried out in a coaxial DBD reactor. The BET and XRD results revealed that the partial substitution of La slightly affected the specific surface area of the catalysts, while the crystalline structure of perovskite were maintained. The $La_{0.8}M_{0.2}MnO_3$ catalysts showed higher ratio of $O_{ads}/(O_{ads}+O_{lat})$ compared to that of pure $LaMnO_3$, whilst the reducibility of the catalysts was improved by doping the catalyst with Ce and Sr only. Among the catalysts, the $La_{0.8}Ce_{0.2}MnO_3$ catalyst exhibited the highest conversion efficiency of ethyl acetate and CO_2 selectivity, indicating the reducibility of the catalysts played an important role in determining the reaction performance of the plasma-catalytic oxidation process.

Acknowledgements

The authors are grateful to the financial support of National Science Fund for National Natural Science Foundation of China (No. 51206143) and the Royal Society (No. RG120591).

References

[1] R. Koppmann, Volatile organic compounds in the atmosphere, John Wiley & Sons2008.
[2] S. Sultana, A. Vandenbroucke, C. Leys, N. De Geyter, R. Morent, Abatement of VOCs with Alternate Adsorption and Plasma-Assisted Regeneration: A Review, Catalysts, 5 (2015) 718-746.
[3] D. Mei, X. Zhu, C. Wu, B. Ashford, P.T. Williams, X. Tu, Plasma-photocatalytic conversion of CO2 at low temperatures: Understanding the synergistic effect of plasma-catalysis, Applied Catalysis B: Environmental, 182 (2016) 525-532.
[4] J.C. Whitehead, Plasma-catalysis: the known knowns, the known unknowns and the unknown unknowns, Journal of Physics D: Applied Physics, 49 (2016) 243001.
[5] A.M. Vandenbroucke, R. Morent, N. De Geyter, C. Leys, Non-thermal plasmas for non-catalytic and catalytic VOC abatement, Journal of Hazardous Materials, 195 (2011)

30-54.
[6] X. Zhu, S. Liu, Y. Cai, X. Gao, J. Zhou, C. Zheng, X. Tu, Post-plasma catalytic removal of methanol over Mn-Ce catalysts in an atmospheric dielectric barrier discharge, Applied Catalysis B: Environmental, 183 (2016) 124-132.
[7] H.-H. Kim, S.-M. Oh, A. Ogata, S. Futamura, Decomposition of gas-phase benzene using plasma-driven catalyst (PDC) reactor packed with Ag/TiO2 catalyst, Applied Catalysis B: Environmental, 56 (2005) 213-220.
[8] Q.H. Trinh, S.B. Lee, Y.S. Mok, Removal of ethylene from air stream by adsorption and plasma-catalytic oxidation using silver-based bimetallic catalysts supported on zeolite, Journal of Hazardous Materials, 285 (2015) 525-534.
[9] Z. Zhang, Z. Jiang, W. Shangguan, Low-temperature catalysis for VOCs removal in technology and application: A state-of-the-art review, Catalysis Today, 264 (2016) 270-278.
[10] X. Zhu, X. Tu, D. Mei, C. Zheng, J. Zhou, X. Gao, Z. Luo, M. Ni, K. Cen, Investigation of hybrid plasma-catalytic removal of acetone over CuO/gamma-Al2O3 catalysts using response surface method, Chemosphere, 155 (2016) 9-17.
[11] Y.J. Lu, Q.G. Dai, X.Y. Wang, Catalytic combustion of chlorobenzene on modified LaMnO3 catalysts, Catalysis Communications, 54 (2014) 114-117.
[12] Y. Wang, Y. Xue, C. Zhao, D. Zhao, F. Liu, K. Wang, D.D. Dionysiou, Catalytic combustion of toluene with La0.8Ce0.2MnO3 supported on CeO2 with different morphologies, Chemical Engineering Journal, 300 (2016) 300-305.
[13] C. Zhou, Z.J. Feng, Y.X. Zhang, L.J. Hu, R. Chen, B. Shan, H.F. Yin, W.G. Wang, A.S. Huang, Enhanced catalytic activity for NO oxidation over Ba doped LaCoO3 catalyst, Rsc Advances, 5 (2015) 28054-28059.
[14] M.T.N. Dinh, J.M. Giraudon, J.F. Lamonier, A. Vandenbroucke, N. De Geyter, C. Leys, R. Morent, Plasma-catalysis of low TCE concentration in air using LaMnO3+δ as catalyst, Applied Catalysis B: Environmental, 147 (2014) 904-911.
[15] A.M. Vandenbroucke, M.T. Nguyen Dinh, N. Nuns, J.M. Giraudon, N. De Geyter, C. Leys, J.F. Lamonier, R. Morent, Combination of non-thermal plasma and Pd/LaMnO3 for dilute trichloroethylene abatement, Chemical Engineering Journal, 283 (2016) 668-675.
[16] M.Q. Shen, Z. Zhao, J.H. Chen, Y.G. Su, J. Wang, X.Q. Wang, Effects of calcium substitute in LaMnO3 perovskites for NO catalytic oxidation, Journal of Rare Earths, 31 (2013) 119-123.
[17] J. Chen, M. Shen, X. Wang, G. Qi, J. Wang, W. Li, The influence of nonstoichiometry on LaMnO3 perovskite for catalytic NO oxidation, Applied Catalysis B: Environmental, 134-135 (2013) 251-257.
[18] C. Zhang, C. Wang, W. Zhan, Y. Guo, Y. Guo, G. Lu, A. Baylet, A. Giroir-Fendler, Catalytic oxidation of vinyl chloride emission over LaMnO3 and LaB0.2Mn0.8O3 (B = Co, Ni, Fe) catalysts, Applied Catalysis B-Environmental, 129 (2013) 509-516.
[19] Z.J. Sui, L. Vradman, I. Reizner, M.V. Landau, M. Herskowitz, Effect of preparation method and particle size on LaMnO3 performance in butane oxidation, Catalysis Communications, 12 (2011) 1437-1441.
[20] X. Zhu, X. Gao, X. Yu, C. Zheng, X. Tu, Catalyst screening for acetone removal in a single-stage plasma-catalysis system, Catalysis Today, 256 (2015) 108-114.

[21] X. Zhu, X. Gao, R. Qin, Y. Zeng, R. Qu, C. Zheng, X. Tu, Plasma-catalytic removal of formaldehyde over Cu-Ce catalysts in a dielectric barrier discharge reactor, Applied Catalysis B: Environmental, 170-171 (2015) 293-300.
[22] J. Wang, Y.G. Su, X.Q. Wang, J.H. Chen, Z. Zhao, M.Q. Shen, The effect of partial substitution of Co in LaMnO3 synthesized by sol-gel methods for NO oxidation, Catalysis Communications, 25 (2012) 106-109.
[23] J.C. Dupin, D. Gonbeau, P. Vinatier, A. Levasseur, Systematic XPS studies of metal oxides, hydroxides and peroxides, Physical Chemistry Chemical Physics, 2 (2000) 1319-1324.
[24] Y. Dai, X.Y. Wang, D. Li, Q.G. Dai, Catalytic combustion of chlorobenzene over Mn-Ce-La-O mixed oxide catalysts, Journal of Hazardous Materials, 188 (2011) 132-139.
[25] D. Mei, X. Zhu, Y.-L. He, J.D. Yan, X. Tu, Plasma-assisted conversion of CO2 in a dielectric barrier discharge reactor: understanding the effect of packing materials, Plasma Sources Science and Technology, 24 (2015) 015011.
[26] E.C. Neyts, K.K. Ostrikov, M.K. Sunkara, A. Bogaerts, Plasma Catalysis: Synergistic Effects at the Nanoscale, Chemical reviews, 115 (2015) 13408-13446.
[27] E.C. Neyts, A. Bogaerts, Understanding plasma catalysis through modelling and simulation—a review, Journal of Physics D: Applied Physics, 47 (2014) 224010.
[28] E.C. Neyts, Plasma-Surface Interactions in Plasma Catalysis, Plasma Chemistry and Plasma Processing, 36 (2015) 185-212.

Figure captions

Fig. 1. XRD patterns of the $La_{0.8}M_{0.2}MnO_3$ catalysts

Fig. 2. XPS spectra of O 1s in the $La_{0.8}M_{0.2}MnO_3$ and $LaMnO_3$ catalysts

Fig. 3. H_2-TPR profiles of the $La_{0.8}M_{0.2}MnO_3$ and $LaMnO_3$ catalysts.

Fig. 4. Effect of $La_{0.8}M_{0.2}MnO_3$ catalysts on plasma-catalytic oxidation of ethyl acetate: (a) oxidation rate; (b) CO_2 selectivity.

Table caption

Table 1 . Physicochemical properties of the catalysts

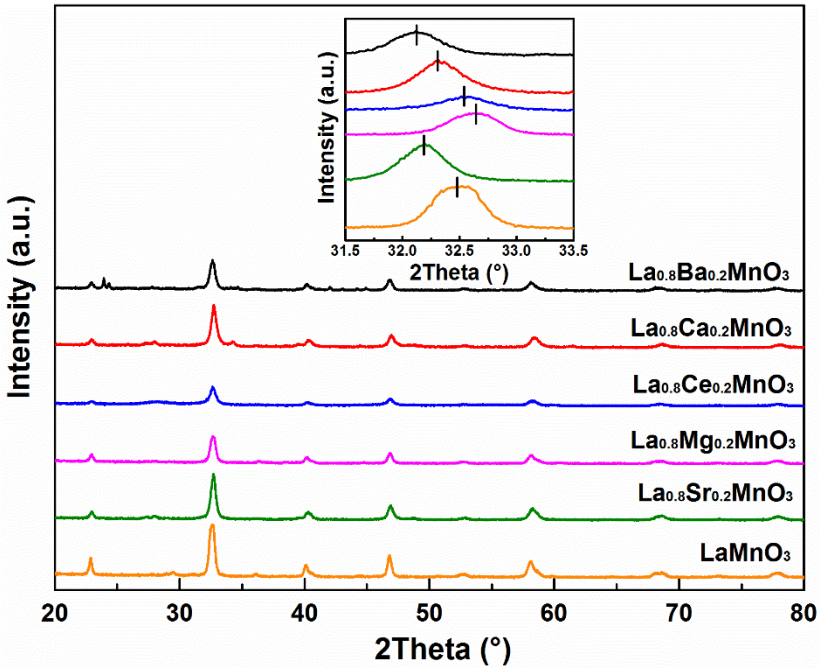
Intensity (a.u.)
2Theta (°)
La0.8Ba0.2MnO3
La0.8Ca0.2MnO3
La0.8Ce0.2MnO3
La0.8Mg0.2MnO3
La0.8Sr0.2MnO3
LaMnO3
20
30
40
50
60
70
80
31.5
32.0
32.5
33.0
33.5

Fig. 1

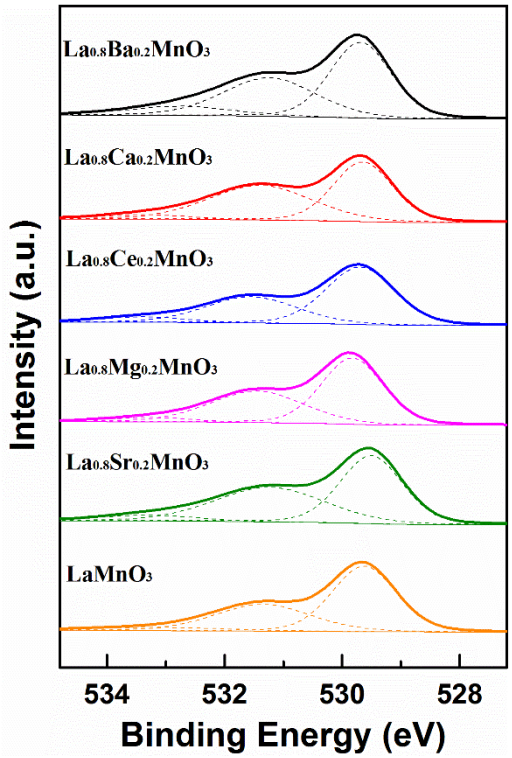
Intensity (a.u.)
La0.8Ba0.2MnO3
La0.8Ca0.2MnO3
La0.8Ce0.2MnO3
La0.8Mg0.2MnO3
La0.8Sr0.2MnO3
LaMnO3
534
532
530
528
Binding Energy (eV)

Fig. 2

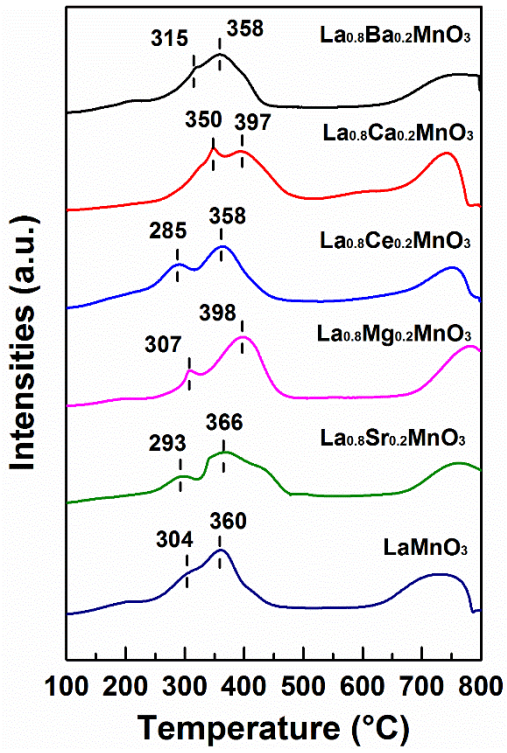
315
358
La0.8Ba0.2MnO3
350
397
La0.8Ca0.2MnO3
285
358
La0.8Ce0.2MnO3
398
307
La0.8Mg0.2MnO3
293
366
La0.8Sr0.2MnO3
304
360
LaMnO3
Intensities (a.u.)
100 200 300 400 500 600 700 800
Temperature (°C)

Fig. 3

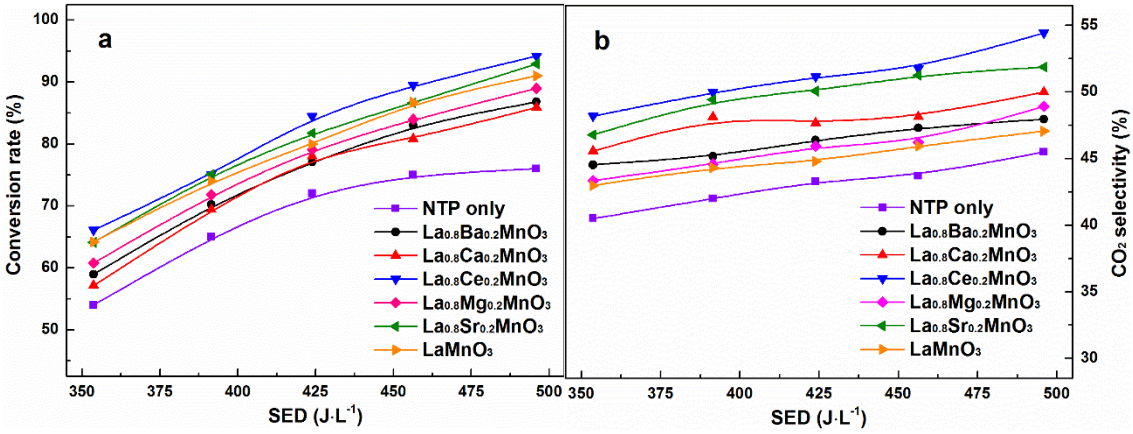
a
b
Conversion rate (%)
CO2 selectivity (%)
SED (J·L-1)
SED (J·L-1)
NTP only
La0.8Ba0.2MnO3
La0.8Ca0.2MnO3
La0.8Ce0.2MnO3
La0.8Mg0.2MnO3
La0.8Sr0.2MnO3
LaMnO3

Fig. 4

Sample	S_{BET} ($m^2 \cdot g^{-1}$)	Pore volume ($cm^3 \cdot g^{-1}$)	Crystallite size (nm)[a]	$O_{ads}/(O_{ads}+O_{lat})$ (%)	H_2 consumption ($\mu mol \cdot g^{-1}$) (T<600 ℃)
$La_{0.8}Ba_{0.2}MnO_3$	11.9	0.097	16.2	38.9	3.73
$La_{0.8}Ca_{0.2}MnO_3$	10.8	0.088	15.9	40.4	4.51
$La_{0.8}Ce_{0.2}MnO_3$	17.0	0.113	14.0	47.5	5.26
$La_{0.8}Mg_{0.2}MnO_3$	12.7	0.086	15.9	42.3	4.02
$La_{0.8}Sr_{0.2}MnO_3$	13.4	0.087	16.6	45.1	3.83
$LaMnO_3$	14.4	0.107	16.8	38.2	3.52

Table 1

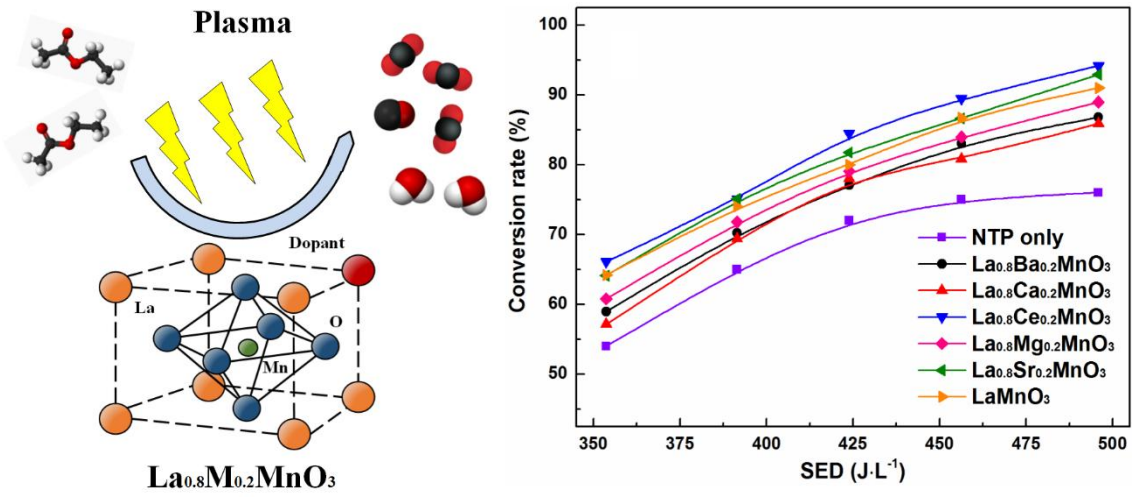

Graphical abstract